ISSN: 0067-2904

Theoretical Study of Density Distributions and Size Radii of ^{8}B and ^{17}Ne

Arkan R. Ridha*, Zaid M. Abbas
Department of physics, College of Science, University of Baghdad, Baghdad, Iraq

Abstract

The proton, neutron and matter density distributions, the corresponding size radii and elastic electron scattering form factors of one-proton ^{8}B and two-proton ^{17}Ne halo nuclei are calculated. The theoretical technique used to fulfill calculations is by assuming that both nuclei under study are composed of two main parts; the first is the compact core and the second is the unstable halo part. The single-particle radial wavefunctions of harmonic-oscillator (HO) and Woods-Saxon (WS) potentials are used to study core and halo parts, respectively. And other approach is studied by using HO potential for both core and halo parts, but using two HO size parameters for both supposed parts. The long tail behavior which is the main characteristic of halo nuclei are well produced for both ^{8}B and ^{17}Ne. The calculated size radii are in general in good agreement with the available experimental data. The electron scattering form factors of the C0+C2 and C0 components are also calculated for ^{8}B and ^{17}Ne, respectively and compared with corresponding stable ^{10}B and ^{20}Ne nuclei. For ^{8}B calculations, the core-polarization (CP) effects are taken into account by using Tassie and Bohr-Mottelson models. The contribution from model-space (MS) part C2 component is taken through pwt interaction. The results of the calculated charge form factors are left for the planned electron-radioactive ion beam colliders where the study of skin or halo on the charge form factors are going to be studied.
PACS number(s): 21.10.Gv, 21.10.Ky, 21.60.Cs, 25.30.Bf

Keywords: halo nuclei, matter density distributions, elastic electron scattering form factors, root-mean square radii, quadrupole moment.

دراسة نظرية لتوزيعات الكثافة وانصاف الاقطار لنوى ^{8}B و ^{17}Ne

اركان رفعه رضا* ، زيد ملك عباس
قسم الفيزياء، كلية العلوم، جامعة بغداد، بغداد، العراق

الخلاصة

تم حساب توزيعات الكثافة البروتونية والنيوترونية والكتلية وانصاف الاقطار المقابلة لها وعوامل التشكل للاستطارة الالكترونية المرنة من نواة الهالة ذات البروتون الواحد ^{8}B ونواة الهالة ذات البروتونين ^{17}Ne . حساباتنا النظرية استندت على تقسيم النواة تحت الدراسة الى جزأين رئيسيين؛ الاول هو جزء القلب المستقر والثاني يمثل جزء الهالة الغير مستقر. الدوال الموجية القطرية لجهد المتذبذب التوافقي البسيط تم استخدامه لدراسة جزء القلب بينما جزء الهالة تم استخدام جهد وودز–ساكسون للنواتين تحت الدراسة. وبطريقة تم استخدام جهد المتذبذب التوافقي لدراسة كلا من جزئي القلب والهالة بأستخدام معامل حجم مختلفين. صفة التذييل الممتد

* Email: arkan_rifaah@yahoo.com

في توزيعات الكثافة الكتلية وهي خاصية مميزة لنوى الهالة تم توليدها بنجاح. انصاف الاقطار المحسوبة كانت على توافق جيد مع تلكم القيم العملية. اخيرا تم حساب عوامل التشكل للاستطارة الالكترونية المرنة لمركبتي (C0+C2) لنواة ^{8}B و (C0) لنواة ^{17}Ne. المركبة C2 في نواة ^{8}B تم حسابها من خلال تأثير استقطاب القلب باستخدام نموذج تاسي ونموذج بور–موتيلسون من خلال تفاعل pwt.

Introduction

The study of nuclear neutron and proton density distributions are essential quantities in understanding both nuclear structure and reactions [1]. The distribution of charge density and charge radii can be measured accurately from high energy electron elastic scattering, but such scattering is so far limited to stable or long-lived isotopes, besides, the measurements of muonic X-rays transitions are precise method for determining charge radii [2]. For unstable isotopes, the measuring of charge radii is available from isotope shift measurements [3]; such measurements have been reported for many elements [4]. Information about matter density distributions are obtained from experiments on elastic hadron scattering [1]. The production of radioactive ion beams which has been started in the mid-eighties enabled the studying both of matter density distributions and matter radii [5,6].

Exotic nuclei are located far from the β-stability line on the chart of nuclides, exhibiting very short life times, mainly due to an unbalanced ratio of proton (Z) and neutron (N) numbers. Exotic nuclei differ remarkably in some other aspects from their stable counterparts, providing us with new insights into understanding atomic nuclei and nuclear forces [7–9]. As experimental data on exotic nuclei are, in general, less abundant than data on stable nuclei, theoretical calculations, interpretations, and predictions play an ever increasing role [10].

Halo nuclei have attracted much attention in the study of nuclear structure over the last three decades [11]. Halos are formed when the valence nucleons tunnel out of the potential barrier to long distances, giving rise to an extended low density tail. This quantum tunneling is possible due to the small binding energy of the valence nucleons for unstable nuclei and also small or no centrifugal barrier conditions. Thus, neutron halos have been prominently observed for neutron rich nuclei. It is however questionable whether proton halos and in particular a two-proton halo can exist due to the presence of the Coulomb barrier [12].

Two main types of halos; the first, two-body halos with one nucleon surrounding the core, like the one-proton halo ^{8}B and the second, Borromean three-body halos with two valence nucleons around the core like ^{17}Ne. The Borromean is defined as a three-body bound system in which any two-body subsystem does not bound. The pairing interaction between the valence neutrons plays an essential role in stabilizing these nuclei [13]. The so called Borromean structure has also been discussed extensively [13, 14].

Knyaz'kov et al [15] extracted and analyzed the *rms* radii of the neutron, proton, and matter distributions for a large group of light exotic nuclei, besides, possible candidates of neutron and proton halo nuclei were discussed. Tel et al [16] the proton, charge and neutron densities, *rms* proton, charge, neutron and matter radii, and neutron skin thickness have been calculated by using Hartree-Fock method for Boron isotopes ($^{7-19}$B). Fan et al [17] has been confirmed that ^{8}B to have a halo structure according to the long tail in the density distribution. For ^{17}Ne, Ozawa et al [18] deduced the effective *rms* radii of the matter distributions for ^{17}N, ^{17}F, and ^{17}Ne using Glauber model calculation. They found an increase in the radii of the proton rich ^{17}F and ^{17}Ne nuclei. Geithner et al [19] have been performed high-precision mass and charge radius measurements on $^{17-22}$Ne, including the proton-halo candidate ^{17}Ne. Tanaka et al [20] have been deduced the density distribution of ^{17}Ne through a modified Glauber model calculation. They found a long tail in the density, consistent with a $(2s_{1/2})^2$ dominant configuration of the two valence protons. In [21] the two-frequency shell model approach is used to calculate the ground proton, neutron and matter density distributions and the corresponding *rms* radii for the ^{17}Ne and ^{27}P nuclei.

In this work, the density distributions, elastic electron charge form factors and size radii for halo ^{8}B and ^{17}Ne nuclei are calculated.

Theoretical formulations

The ground point density distributions of neutrons and protons can be written as [22]:

$$\rho_{t_z=n/p}(r) = \rho^{c}_{t_z=n/p}(r) + \rho^{h}_{t_z=n/p}(r) \quad (1)$$

where t_z is the projection of the isospin quantum number ($t_z = \frac{1}{2} = p$ for protons and $t_z = -\frac{1}{2} = n$ for neutrons). $\rho^c_{n/p}(r)$ is the density distribution of the core neutrons/protons calculated using the radial wavefunctions of harmonic-oscillator (HO) potential ($R_{nl}(r)$) [23] as follows:

$$\rho^c_{n/p}(r) = \frac{1}{4\pi}\sum_{nl} X^{nl,core}_{n/p} \left|R_{nl}(r, b_{n/p})\right|^2 \quad (2)$$

In Eq. (2), $X^{nl,core}_{n/p}$ is the number of neutrons/protons in the nl shell. n and l represent the principal and orbital quantum numbers, respectively. $b_{n/p}$ is the HO size parameter of neutrons/protons. The summation in Eq. (2) spans all occupied orbits in the core for both nuclei under study. The matter density distribution for core can be written as a sum the densities of core neutrons and protons ($\rho^c_m(r) = \rho^c_p(r) + \rho^c_n(r)$). In Eq. (1), $\rho^h_{n/p}(r)$ represents the density distribution of halo neutrons/protons and it is calculated by using WS radial wave functions and can be written as:

$$\rho^h_{n/p}(r) = \frac{1}{4\pi} X^{nlj,halo}_{n/p} \left|R_{nlj,t_z}(r)\right|^2 \quad (3)$$

where

$$X^{nlj,halo}_{n/p} = N^{halo}_{t_z} \sum_{nlj} a_{nlj} \quad (4)$$

In Eq. (3) and (4), $N^{halo}_{t_z}$ and $X^{nlj,halo}_{n/p}$ are the occupation numbers and fractional occupation numbers of neutrons/protons, respectively in the sub-shell nlj, where j represents the total angular quantum number. Besides, a_{nlj} represents the probability number for the existence of halo nucleons in the higher sub-shells. The radial wave functions of WS potential $R_{nlj,t_z}(r)$ are found from the solution to the second rank differential equation of the radial part of Schrödinger equation [24]:

$$\left(\frac{\hbar^2}{2\mu}\frac{d^2}{dr^2} - v(r) - \frac{l(l+1)\hbar^2}{2\mu r^2} + \varepsilon_{nlj,t_z}\right) R_{nlj,t_z}(r) = 0 \quad (5)$$

$\mu = m_{t_z}(A-1)/A$ is the reduced mass of the core $(A-1)$ and single nucleon, m_{t_z} is the mass of nucleon, A is the atomic mass and ε_{nlj,t_z} is the binding energy of single halo nucleon.

In Eq. (5), the local potential $v(r)$ can be written in the following compact form [25, 26]:

$$v(r) = v_{cent}(r) + v_{s.o.}(r) + v_c(r) \quad (6)$$

In Eq. (6), $v_{cent}(r)$ represents the central part and can be written as:

$$v_{cent}(r) = \frac{-U_0}{\left(1+e^{\left(\frac{r-R}{a}\right)}\right)} \quad (7)$$

where U_0 is the depth of central part, a is the diffuseness and $R = r_0(A-1)^{1/3}$ is the radius parameter. $v_{s.o.}(r)$ in Eq. (6), represents the spin-orbit part and is defined as:

$$v_{s.o.}(r) = \left(\frac{\hbar}{m_\pi c}\right)^2 \frac{U_{s.o.}}{r}\frac{d}{dr}\frac{1}{\left(1+e^{\left(\frac{r-R_{s.o.}}{a_{s.o.}}\right)}\right)}\langle \hat{l}.\hat{\sigma}\rangle = -\left(\frac{\hbar}{m_\pi c}\right)^2 \frac{U_{s.o.}}{r}\frac{e^{\left(\frac{r-R_{s.o.}}{a_{s.o.}}\right)}}{\left(1+e^{\left(\frac{r-R_{s.o.}}{a_{s.o.}}\right)}\right)^2}\langle \hat{l}.\hat{\sigma}\rangle \quad (8)$$

where m_π is the pion mass ($m_\pi c^2 = 139.57\ MeV$), $\hbar c = 197.33\ MeV\ fm$, $\left(\frac{\hbar c}{m_\pi c^2}\right)^2 \approx 2\ fm^2$, $U_{s.o.}$ is the strength or depth of spin-orbit potential, $a_{s.o.}$ is the diffuseness of spin-orbit part, $R_{s.o.} = r_{S.O.}(A-1)^{1/3}$ is the radius parameter of spin-orbit. $\hat{l}$ and $\hat{\sigma}$ are the angular momentum operator and the Pauli Matrices respectively and the matrix element of their product can be written as:

$$\langle \hat{l}.\hat{\sigma}\rangle = \begin{cases} -\frac{1}{2}(l+1) & for\ j = l - \frac{1}{2} \\ \frac{1}{2}l & for\ j = l + \frac{1}{2} \end{cases}$$

The last term in Eq. (6) $v_c(r)$ indicates the Coulomb potential generated by a homogeneous charged sphere and can be written for protons as [27]:

$$v_C(r) = \begin{cases} (Z-1)\frac{e^2}{r} & if\ r > R \\ \frac{(Z-1)e^2}{2R}\left[3 - \frac{r^2}{R^2}\right] & if\ r < R \end{cases}, \quad (9)$$

$v_C(r) = 0$ for neutrons, with $e^2 = 1.44\ MeV.fm$.

Finally, Eq. (6) can be written as:

$$v(r)=\frac{-U_0}{\left(1+e^{\left(\frac{r-R}{a}\right)}\right)}-\left(\frac{\hbar}{m_\pi}\right)^2\frac{1}{r}\frac{U_{S.O.}}{a_{S.O.}}\frac{e^{\left(\frac{r-R_{S.O.}}{a_{S.O.}}\right)}}{\left(1+e^{\left(\frac{r-R_{S.O.}}{a_{S.O.}}\right)}\right)^2}\langle\hat{l}.\hat{\sigma}\rangle+v_C(r) \quad (10)$$

The charge density distribution ($\rho_{ch}(r)$) (CDD) is obtained by folding the charge density of the single proton ($\rho_{pr}(r)$) into the density distribution of point protons calculated in Eq. (1) as follows [25]:

$$\rho_{ch}(r)=\int\rho_p(r)\rho_{pr}(\boldsymbol{r}-\boldsymbol{r'})d\boldsymbol{r'} \quad (11)$$

$\rho_p(\vec{r})$ can be written as [25]:

$$\rho_{pr}(r)=\frac{1}{\left(\sqrt{\pi}a_{pr}\right)^3}e^{\left(\frac{-r^2}{a_{pr}^2}\right)} \quad (12)$$

where $a_{pr}=0.65\ fm$ [23]. The value of a_{pr} reproduces the experimental rms charge radius of the proton, $\langle r^2\rangle_{pr}^{1/2}=\left(\frac{3}{2}\right)^{1/2}a_{pr}\approx 0.8\ fm$ [23].

The ground density distributions of point neutrons and protons for stable nuclei can be found from:

$$\rho_{n/p}(r)=\frac{1}{4\pi}\sum_{nl}X_{n/p}^{nl}\,|R_{nl}(r)|^2 \quad (13)$$

The rms radii of neutron, proton, charge and matter can be directly calculated from [25]:

$$\langle r^2\rangle_X^{1/2}=\sqrt{\frac{4\pi}{X}\int_0^\infty\rho_X(r)r^2dr} \quad (14)$$

In Eq. (14), X denotes to N (number of neutrons), Z (atomic number which is the same for proton and charge) and (A), respectively.

In the first Born approximation, the longitudinal electron scattering form factors can be found from [28, 29]:

$$\left|F_J^C(q)\right|^2=\frac{4\pi}{Z^2(2J_i+1)}\left|\langle J_f\|\boldsymbol{\mathcal{O}}_J^C(q)\|J_i\rangle\right|^2 \quad (15)$$

where q is the momentum transfer from electron to nucleus during scattering. Eq. (15) can be simplified to the following [30]:

$$\left|F_J^C(q)\right|^2=\frac{4\pi}{Z^2(2J_i+1)}\left|\int_0^\infty j_J(qr)\,\rho_{ch,J}(r)r^2dr\right|^2 \quad (16)$$

where $j_J(qr)$ and $\rho_{ch,J}(r)$ are spherical Bessel function and charge transition density distribution, respectively.

The total longitudinal form factors are given by:

$$|F(q)|^2=\sum_J\left|F_J^C(q)\right|^2 \quad (17)$$

For small q leading to photon point ($q=w=\frac{E_x}{\hbar c}$), E_x is the excitation energy, the spherical Bessel function can be written as:

$$j_J(qr)=\frac{(qr)^J}{(2J+1)!!}\left(1-\frac{(qr)^2}{2(2J+3)}+\cdots\right)\approx\frac{(qr)^J}{(2J+1)!!} \quad (18)$$

The Coulomb form factor in Eq. (16) can be reduced to:

$$\left|F_J^C(q=w)\right|^2=\frac{4\pi}{Z^2(2J_i+1)}\left(\frac{q^J}{(2J+1)!!}\right)\left|\int_0^\infty\rho_{ch,J}(r)\,r^{J+2}dr\right|^2$$

which can be written in terms of the matrix element of the electric multipole operator as follows:

$$\left|F_J^C(q=w)\right|^2=\frac{4\pi}{Z^2(2J_i+1)}\left(\frac{q^J}{(2J+1)!!}\right)^2\left|\langle J_f\|\boldsymbol{\mathcal{O}}_J\ (\vec{r})\|J_i\rangle\right|^2 \quad (19)$$

From Eq. (19), the multiparticle reduced matrix element of electric multipole operator can be written as:

$$\langle J_f\|\boldsymbol{\mathcal{O}}_J\ (\vec{r})\|J_i\rangle=Z\frac{(2J+1)!!}{q^J}\sqrt{\frac{(2J_i+1)}{4\pi}}F_J^C(q=w) \quad (20)$$

The quadrupole moment is related to the multiparticle reduced matrix element of electric multipole operator by the relation [27]:

$$Q=\sqrt{\frac{16\pi}{5}}\begin{pmatrix}J & 2 & J\\ -J & 0 & J\end{pmatrix}\langle J_f\|\boldsymbol{\mathcal{O}}_J\ (\vec{r})\|J_i\rangle \quad (21)$$

The quadrupole moment can be reduced to the following final formula:

$$Q = \sqrt{\frac{16\pi}{5}} \begin{pmatrix} J & 2 & J \\ -J & 0 & J \end{pmatrix} \frac{(2J+1)!!Z}{q^J} \sqrt{\frac{(2J_i+1)}{4\pi}} F^C_{J=2}(q=w) \quad (22)$$

In Eq. (16), the transition density distribution is coming from the contribution of core-polarization (CP) and model-space (MS) as follows [31]:

$\rho_{ch,J}(r) = \rho^{CP}_{ch,J}(r) + \rho^{MS}_{ch,J}(r)$

In the present work, $\rho^{CP}_{ch,J}(r)$ is calculated using Tassie [32- 34] and Bohr-Mottelson [35] models, respectively as:

$$\rho_{ch,J}(r) = Ar^{J-1}\frac{d}{dr}\rho_{ch}(r) \quad (23)$$

and

$$\rho_{ch,J}(r) = A\frac{d}{dr}\rho_{ch}(r) \quad (24)$$

where, A in the above two equations are chosen so as to reproduce the experimental quadrupole moments.

$\rho^{MS}_{J,t_z}(r)$ can be written as [36]:

$$\rho^{MS}_{J,t_z}(r) = \frac{1}{\sqrt{4\pi}}\frac{1}{\sqrt{2J_i+1}}\sum_{ab} X^{J_f\ J_i\ ,J}_{a,b,t_z} \left\langle j_a \middle|\middle| Y_J \middle|\middle| j_b \right\rangle\ R_{n_a l_a j_a, t_z}(r) R_{n_b l_b j_b, t_z}(r) \quad (25)$$

where $X^{J_f\ J_i\ ,J}_{a,b,t_z}$ is the proton or neutron one body density matrix element and a and b stand for the single-particle states.

The incoherent sum of the longitudinal form factor for ground C0 and C2 parts can be written as:

$$|F(q)|^2 = \left|F^C_0(q)\right|^2 + \left|F^C_2(q)\right|^2 \quad (26)$$

The CDD ($\rho_{ch}(r)$) coming from the contributions of one proton in the model-space is obtained by using the technique mentioned in Eq. (11). The CDD coming from the contributions of neutrons in the model-space is obtained by folding the charge density of single neutron ($\rho_{neu}(r)$) into the density distribution of the point neutrons ($\rho^{MS}_{J,n}(r)$) calculated in Eq. (25) as follows [37]:

$$\rho_{ch}(r) = \int \rho^{MS}_{J,n}(r)\rho_{neu}(\boldsymbol{r}-\boldsymbol{r'})d\boldsymbol{r'} \quad (27)$$

where $\rho_{neu}(\vec{r})$ is chosen to take the following form [34]:

$$\rho_{neu}(r) = \sum_1^2 \frac{\theta_i}{(\pi r_i^2)^{3/2}} e^{-r^2/r_i^2} \quad (28)$$

The parameters θ_i and r_i are given in Table-1.

Table 1-Parameter of the neutron CDD

θ_1	1
θ_2	-1
r_1^2 (fm^2)	0.469
r_2^2 (fm^2)	0.546

The binding energies of the single proton/neutron in HO potential can be written as [23, 27]:

$$E_{nljt_z} = -V_0 + \left(N+\frac{3}{2}\right)\hbar\omega_{t_z} + \left\langle nljm_j t t_z \middle| V_{ls}(r) \middle| nljm_j t t_z \right\rangle \quad (29)$$

where $N = 2n + l - 2$ (is the number of quanta in the oscillator) and $\hbar\omega_{t_z} = \frac{(\hbar c)^2}{m_{t_z} c^2 b_{t_z}^2}$. In Eq. (29), the matrix element to the spin-orbit interaction can be written as:

$$\left\langle nljm_j t t_z \middle| V_{ls}(r) \middle| nljm_j t t_z \right\rangle = \langle f(r)\rangle_{nl} \begin{cases} \frac{-(2l+1)}{2}, & for\ j = l+\frac{1}{2} \\ \frac{l}{2}, & for\ j = l-\frac{1}{2} \end{cases} \quad (30)$$

The matrix element to the radial part of the spin-orbit interaction can takes the following form [23, 27]:

$$\langle f(r)\rangle_{nl} = \langle nl|f(r)|nl\rangle \approx -20A^{\frac{-2}{3}}\ \text{MeV} \quad (31)$$

Results and discussions

In the present work, the MDDs, rms proton, charge, neutron, and matter radii, besides elastic electron scattering charge form factor, are computed using the radial wave functions of HO potential for core part for all nuclei under study, the halo part are computed using the radial wave function of WS potential. Regarding the core part, two HO size parameters are used, one for protons (b_p) and the second for neutrons (b_n) in order to regenerate the available experimental rms radii.

The depth of central part of WS potential(U_0) in this work is chosen so as to reproduce the experimental single-nucleon separation energies for ^{8}B (S_p) and ^{17}Ne ($S_p = S_{2p}/2$) (see Table 2), while other parameters in Eq. (8) are fixed to be $U_{s.o.} = 10\ MeV,\ \ a_0 = a_{s.o.} = 0.6\ fm$, $r_0 = r_{S.O.} = R_C = 1.2\ fm$.

For halo ^{8}B and ^{17}Ne nuclei, the chosen size parameters of HO potential of protons and neutrons in the core and the parameters of WS potential of halo nucleon(s) are presented in Table-2. The fractional occupation numbers ($X_{n/p}^{nlj,halo}$) are related to the probability of occupation (a_{nlj}) and calculated by using Eq. (4). The configuration mixing is chosen to be between the subshells, $1p_{3/2}$ and $1p_{1/2}$ for ^{8}B and among $1d_{5/2}$, $2s_{1/2}$ and $1d_{3/2}$ for ^{17}Ne as shown in Table-2.

The computed rms proton, charge, neutron, and matter radii are presented in Table 3, for the nuclei under study. The computed results of the rms charge and matter radii are well predicted for the nuclei under study.

Table 2-HO and WS parameters for core and halo for nuclei

nucleus	HO size parameters for core (fm)	nl_j	Occupation percentage (a_{nlj})	$U_0(MeV)$	Separation energies of halo nucleons (MeV) [38]
$^{8}_{5}B_3$	$b_n = 1.6$ $b_p = 1.636$	$1p_{3/2}$	84%	44.11588	$S_p = 0.13639 \pm 0.001$
		$1p_{1/2}$	16%	63.13901	$S_p = 0.13639 \pm 0.001$
$^{17}_{10}Ne_7$	$b_n = 1.64$ $b_p = 1.66$	$1d_{5/2}$	10 %	54.13079	$S_{2p} = 0.9331 \pm 0.00061$ $S_p = 0.467$
		$2s_{1/2}$	80 %	59.97527	$S_p = 0.467$
		$1d_{3/2}$	10 %	74.78185	$S_p = 0.467$

Table 3-The calculated $\langle r^2\rangle_{ch}^{1/2}$, $\langle r^2\rangle_{p}^{1/2}$, $\langle r^2\rangle_{n}^{1/2}$, and $\langle r^2\rangle_{m}^{1/2}$

nucleus	Model	$\langle r^2\rangle_{ch}^{1/2}$ (fm)	Exp. $\langle r^2\rangle_{ch}^{1/2}$ (fm)	$\langle r^2\rangle_{p}^{1/2}$ (fm)	Exp. $\langle r^2\rangle_{p}^{1/2}$ (fm)	$\langle r^2\rangle_{n}^{1/2}$ (fm)	$\langle r^2\rangle_{m}^{1/2}$ (fm)	Exp. $\langle r^2\rangle_{m}^{1/2}$ (fm)
$^{8}_{5}B_3$	HO+WS	2.819	2.82 $\pm$0.06 [39]	2.708	2.76 $\pm$ 0.08 [40]	2.166	2.519	2.55 $\pm$ 0.08 [40]
	HO+HO	2.771		2.655		2.328	2.537	
$^{17}_{10}Ne_7$	HO+WS	3.049	3.0413 [41]	2.955	-	2.44	2.75	2.75(7) [42]
	HO+HO	3.049		2.944		2.42	2.742	

The calculated MDDs are shown in Figure-1 and compared with experimental data. The solid and dashed curves represent the calculated MDDs for nuclei under study using HO+WS and HO+HO, respectively. In Figure- 1(a) for ^{8}B, it is clear from such figure that there is a very good agreement with experimental data. The result of HO+HO is completely failed to predict the data. The difference between the neutron and proton rms radii is $|R_n - R_p| = |2.166 - 2.708| = 0.542\ fm$ (0.6± 0.08 [40]). In Figure- 1(b), a very good agreement is obtained between calculated and experimental MDDs for ^{17}Ne on contrary to the results of HO+HO which again failed to predict the data. The difference between neutron and proton rms radii is $|R_n - R_p| = |2.44 - 2.944| = 0.504\ fm$; this provides an additional evidence for the halo structure in such nucleus.

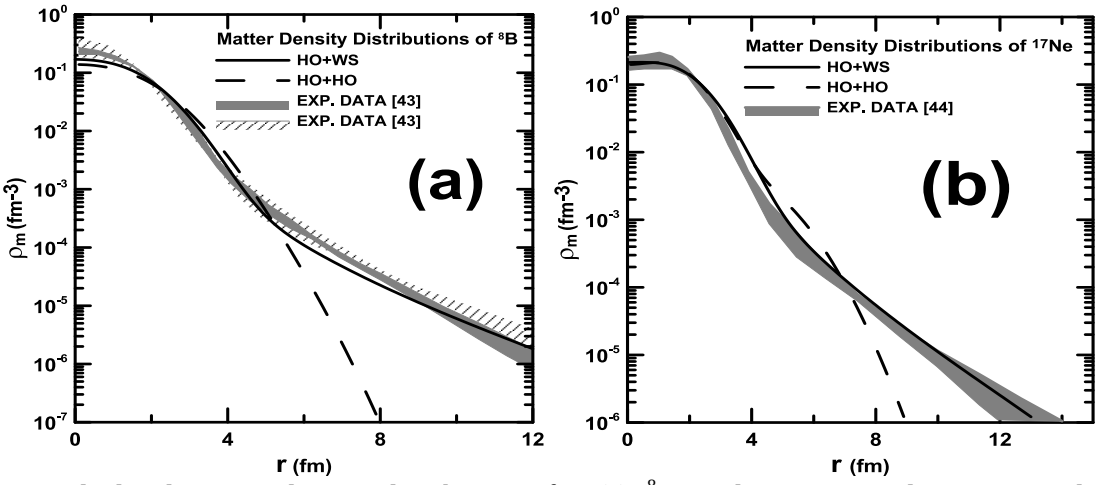

Figure1-Calculated matter density distributions for (a) ^{8}B nucleus compared experimental data represented by hatched and shaded area [43] (b) ^{17}Ne nucleus compared experimental data represented by shaded area [44].

In Figure-2, the proton and neutron density distributions for both nuclei (Figure- 1(a) for ^{8}B and Figure- 1(b) for ^{17}Ne) are presented by solid and dashed curves, respectively (only for HO+WS results). The long tail is remarkably observed in the proton distributions in both nuclei indicating the existence of 1p-halo for ^{8}B and 2p-halo for ^{17}Ne.

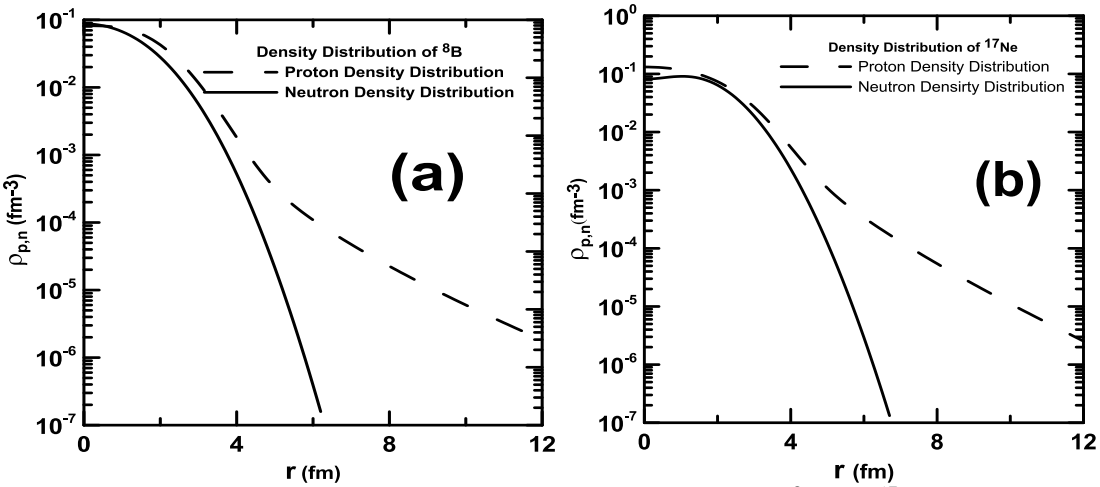

Figure 2-Neutron and proton density distributions for ^{8}B and ^{17}Ne.

The logarithm of the ratio of proton over neutron density distributions are depicted in in Figure-3(a) for ^{8}B and 3(b) for ^{17}Ne. The deviation between protons and neutrons distributions is clearly observed especially in ^{8}B.

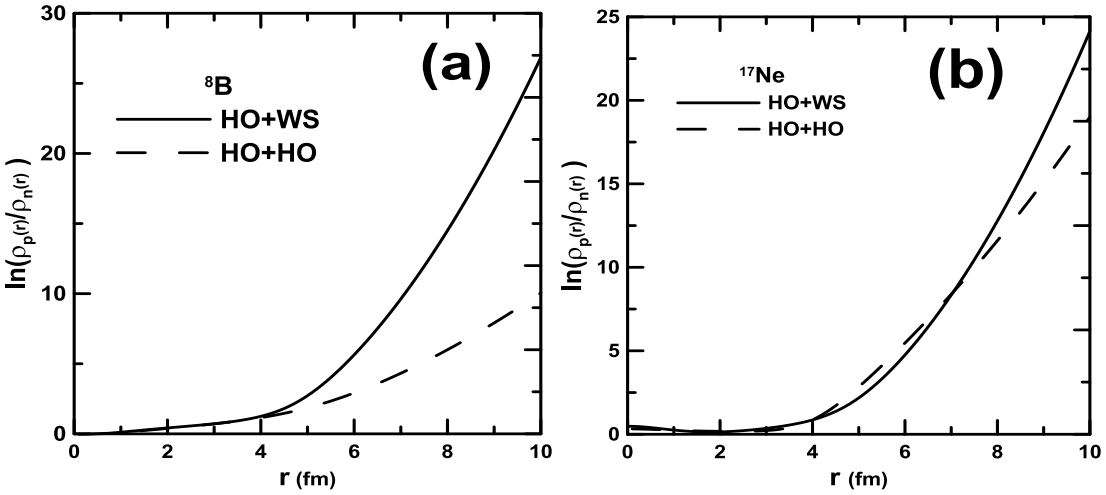

Figure 3-Logarithm of the ratio of proton over neutron density distributions.

The calculated elastic electron scattering charge form factors are illustrated in Figure- 4(a) for ^{8}B and 4(b) for ^{17}Ne, respectively, and compared with experimental data of the corresponding stable ^{10}B and ^{20}Ne nuclei, respectively. For ^{8}B, the solid and dashed curves represent the calculated charge form factor of C0+C2 components using Tassie and Bohr-Mottelson models, respectively. The pwt interaction [45] is used to obtain the one-body density matrix elements (OBDM) needed to accomplish the calculations, where the core of such interaction is $(1s_{1/2})^4$ and the model-space is the full 1p-shell.
For neutrons a_n=0.6 fm, $r_0 = 1.2$ fm, V_{ls}= 10 MeV, the central depths are chosen to be, $V_{0(n)}\left(1p_{\frac{3}{2}}\right) = 81.87\ MeV$ and $V_{0(n)}\left(1p_{\frac{1}{2}}\right) = 85.16\ MeV$, $V_0(n)$ in order to regenerate the corresponding single neutron binding energies, $\varepsilon_n\left(1p_{\frac{3}{2}}\right) = -19.77\ MeV$ and $\varepsilon_n\left(1p_{\frac{1}{2}}\right) = -12.267\ MeV$. For protons a_n=0.8 fm , $r_0 = 1.208$ fm, V_{ls}= 10 MeV, the central depths are chosen to be, $V_{0(p)}\left(1p_{\frac{3}{2}}\right) = 62.82\ MeV$ and $V_{0(p)}\left(1p_{\frac{1}{2}}\right) = 57.32\ MeV$ in order to regenerate the corresponding single proton binding energies, $\varepsilon_p\left(1p_{\frac{3}{2}}\right) = -7.636\ MeV$ and $\varepsilon_p\left(1p_{\frac{1}{2}}\right) = -0.136\ MeV$ for higher subshells. Such single proton/neutron binding energies are predicted by using Eq. (29) with $V_{0(p)} = -45.761\ MeV$ and $b_p = 1.867\ fm$ for protons and $V_{0(n)} = -57.892\ MeV$ and $b_n = 1.6\ fm$ for neutrons.
The normalization constant in Eq. (26) and (27) are computed using the CDD of HO+WS so as to reproduce the experimental quadrupole moments of ^{8}B ($6.43 \pm 0.14\ efm^2$) [46]. In Figure- 4(b), the solid and dashed curves represent the calculated charge form factor of the C0 component in HO+WS and HO+HO, respectively. It is clear from aforementioned both figures that the results of HO+WS shift the results to approach experimental data, on contrary to the results of HO+HO which underestimate the calculated charge form factors.

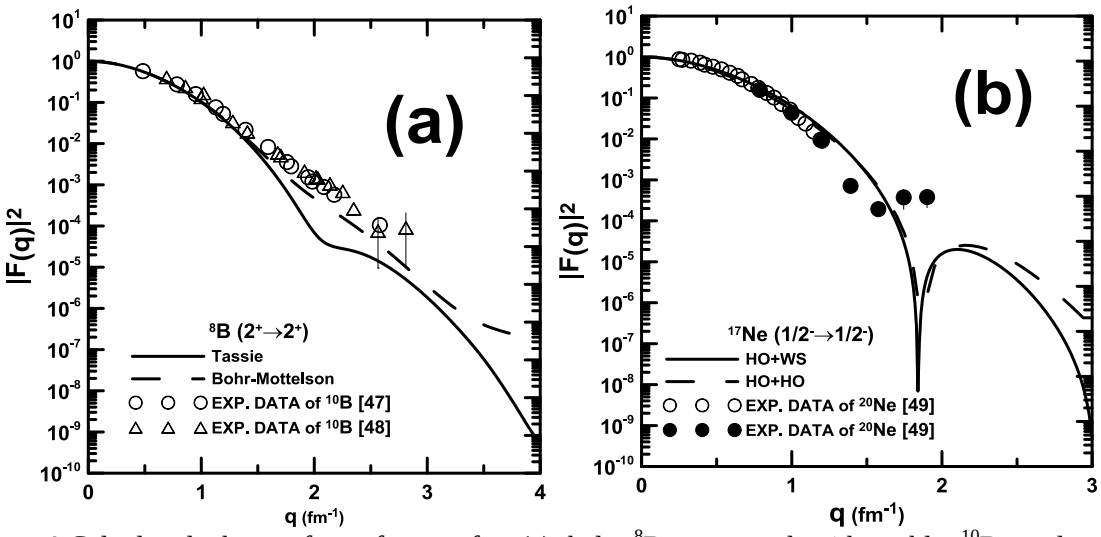

Figure 4-Calculated charge form factors for (a) halo ^{8}B compared with stable ^{10}B nucleus are represented by empty circles [47] and triangles [48] (b) halo ^{17}Ne nucleus compared with stable ^{20}Ne nucleus are by empty and filled circles are taken from [49].

Conclusion

The density distributions of protons, neutron and nucleons, the corresponding *rms* radii and elastic electron scattering form factors of one-proton halo in ^{8}B, and two-proton halo in ^{17}Ne are calculated. The core and halo parts of both nuclei are studied by using the radial wavefunctions of harmonic-oscillator (HO) and Woods-Saxon potential (WS) potentials, respectively. The long tail in the calculated matter density distributions is well generated. The calculated *rms* radii are in good agreements with available experimental data. The C0 and C0+C2 components of the elastic Coulomb electron scattering form factors for ^{17}Ne and ^{8}B, respectively are also calculated. The C2 component in ^{8}B is studied by taking into account the core-polarization effect by using Tassie and Bohr-Mottelson models. The contribution from model-space (MS) is calculated by using pwt interaction. The results of the calculated elastic charge form factors are controversial till future experiments on the electron-radioactive beam colliders are conducted. It is concluded that the HO+WS is capable of reproducing information about the nuclear structures of the halo nuclei as do those of the experimental data.

References

1. Batty, C. J., Friedman, E., Gils, H. J. and Rebel, H. **1989**. Experimental methods for studying nuclear density distributions. *Advances in Nuclear Physics*, **19**: 1–188.
2. Uberall, H. **1971**. *Electron Scattering from Complex Nuclei*, Part A (Academic Press, New York, 1971) Chapter 5.
3. Otten, W. E. **1987.** *Nuclear Radii and Moments of Unstable Isotope, Treatise of Heavy-Ion Physics*. Vol. 8, Plenum Press, New York.
4. Angeli, I.and Marinova, K. P. **2013**. Table of experimental nuclear ground state charge radii: An update. *Atomic Data and Nuclear Data Tables*, **99**: 69-95.
5. Tanihata, I. **1985**. Nuclear physics using unstable nuclear beams. *Hyperfine Interactions*, **21**: 251-264.
6. Tanihata, I., Hamagaki, H., Hashimoto, O., Nagamiya, S., Shida, Y., Yoshikawa, N., Yamakawa, O., Sugimoto, K., Kobayashi, T., Greiner, D.E., Takahashi, N. and Nojiri, Y. **1985**. Measurements of interaction cross sections and radii of He isotopes. *Phys. Lett. B,* **160**: 380-384.
7. Sorlin, O. and Porquet, M.G. **2008**. Nuclear magic numbers: new features far from stability. Prog. *Part. Nucl. Phys*. **61**: 602-673.
8. Gade, A. and Glasmacher, T. **2008**. In-*beam* nuclear spectroscopy of bound states with fast *exotic* ion *beams*. *Prog. Part. Nucl. Phys.* **60**: 161.

9. Otsuka, T. **2013**. Exotic nuclei and nuclear forces. *Phys. Scr*. **T152**: 014007.

10. Tsunoda, N., Otsuka, T., Shimizu, N., Hjorth-Jensen, M., Takayanagi, K. and Suzuki, T. **2017**. Exotic neutron-rich medium-mass nuclei with realistic nuclear forces. *Phys. Rev. C*, **95**: 021304(R) 1-6

11. Tanihata, I. **1996.** Neutron halo nuclei. *J. Phys G: Nucl. Part Phys*. **22**: 157-198.

12. Kanungo, R. **2004**. Two-proton halo in 17Ne. *Nuclear Physics A*, **738**: 293-297.

13. Bertsch, G.F. and Esbensen, H. **1991**. Pair correlations near the neutron drip line. *Ann. Phys*. **209**: 327-363.

14. Zhukov, M.V., Danilin, B.V., Fedorov, D.V., Bang, J.M., Thompson, I.J. and Vaagen, J.S. **1993**. Bound state properties of Borromean halo nuclei: ^{6}He and ^{11}Li. *Phys. Rep*. **231**: 151-199.

15. Knyaz'kov, O. M., Kukhtina, I. N. and Fayans, S. A. **1999**. Interaction cross sections and structure of light exotic nuclei. *Physics of Particles and Nuclei*, **30**: 369-385.

16. Tel, E., Okuducu, S., Tanir, G., Akti, N. N. and Bolukdemir, M. H. **2008**. Calculation of Radii and Density of $^{7-19}$B Isotopes Using Effective Skyrme Force. *Commun. Theor. Phys*. **49**: 696-702.

17. Fan, G.W., Fukuda, M., Nishimura, D., Cai, X.L., Fukuda, S., Hachiuma, I., Ichikawa, C., Izumikawa, T., Kanazawa, M., Kitagawa, A., Kuboki, T., Lantz, M., Mihara, M., Nagashima, M., Namihira, K., Ohkuma, Y., Ohtsubo, T., Ren, Z., Sato, S., Sheng, Z.Q., Sugiyama, M., Suzuki, S., Suzuki, T., Takechi, M., Yamaguchi, T. and Xu, W. **2015**. Density distribution of ^{8}Li and ^{8}B and capture reaction at low energy. *Phys. Rev*. **C91**: 014614 (1-5).

18. Ozawa, A., Kobayashi, T., Sato, H., Hirata, D., Tanihata, I., Yamakawa, O., Omata, K., Sugimoto, K., Olson, D., Christie, W. and Wieman, H. **1994**. Interaction cross-sections and radii of mass number A = 17 isobars (N-17, F-17 and Ne-17. *Phys. Lett*. *B***, 334**: 18-22.

19. Geithner, W., Neff, T., Audi, G., Blaum, K., Delahaye, P., Feldmeier, H., George, S., Guénaut, C., Herfurth, F., Herlert, A., Kappertz, S., Keim, M., Kellerbauer, A., Kluge, H. J., Kowalska, M., Lievens, P., Lunney, D., Marinova, K., Neugart, R., Schweikhard, L., Wilbert, S., and Yazidjian, C. **2008**. Masses and Charge Radii of $^{17-22}$Ne and the Two-Proton-Halo Candidate ^{17}Ne. *Phys. Rev. Lett*. **10**: 252502 (1-4).

20. Tanaka, K., Fukuda, M., Mihara, M., Takechi, M., Nishimura, D., Chinda, T., Sumikama, T., Kudo, S., Matsuta, K., Minamisono, T., Suzuki, T., Ohtsubo, T., Izumikawa, T., Momota, S., Yamaguchi, T., Onishi, T., Ozawa, A., Tanihata, I. and Zheng, T. **2010**. Density distribution of Ne-17 and possible shell-structure change in the proton-rich sd-shell nuclei. *Phys. Rev*. *C***, 82**: 044309 (1-11).

21. [Hamoudi, A. K., Radhi, R. A. and Ridha, A. R. **2015**. Elastic electron scattering from ^{17}Ne and ^{27}P exotic nuclei. *Iraqi Journal of Physics*, **13**: 68-81.

22. Hamoudi, A. K., Radhi, R. A. and Ridha, A. R. **2012**. Theoretical study of matter density distribution and elastic electron scattering form factors for the neutron-rich ^{22}C exotic nucleus. *Iraqi Journal of Physics*, **10**: 25-34.

23. Brussard, A. P. J.and Glademans, P. W. M. **1977**. *Shell-model Application in Nuclear Spectroscopy*. North-Holland Publishing Company, Amsterdam.

24. Brown, B. A., Massen, S. E. and Hodgson, P. E. **1979**. Proton and neutron density distributions for A=16-58 nuclei. *Journal of Physics G*, **5**: 1655-1698.

25. Elton, L. R. B. and Swift, A. **1967**. Single-particle potentials and wave functions in the 1p and 2s-1d shells. *Nuclear Physics A***, 94**: 52-72.

26. Gamba, S., Ricco, G. and Rottigni, G. **1973**. A phenomenological woods-saxon potential for p-shell nuclei. *Nuclear Physics A***, 213**: 383-396.

27. Ring, P. and Schuck, P. **1981**. *The Nuclear Many-Body Problem*. Springer-Verlag.

28. deforest, T. Jr. and Walecka, J. D. **1966**. Electron scattering and nuclear structure. *Advances in Physics*, **15**: 1-109.

29. Brown, B. A., Wildenthal, B. H., Williamson, C. F., Rad, F. N., Kowalski, S., Crannell, H. and O'Brien, J. T. **1985**. Shell-model analysis of high-resolution data for elastic and inelastic electron scattering on ^{19}F. *Physical Review C***, 32**: 1127-1145.

30. Radhi, R. A., Hamoudi, A. K. and Salman, Z. A. **2009**. The Calculation of the Charge Density Distributions and the Longitudinal Form Factors of ^{10}B Nucleus by Using the Occupation Numbers of the States. *Iraqi Journal of Physics*, **7**(10): 11-18.

31. Xiangdong Ji and Wildenthal, B. H. **1988**. Shell-model predictions for electromagnetic properties of N=50 nuclei. *Phys. Riv. C,* **38**: 2849-2859.
32. Brown, B. A., Arima, A. and McGrory, J. B. **1977**. E2 core-polarization charge for nuclei near ^{16}O and ^{40}Ca. *Nuclear Physics A,* **277**: 77-108.
33. Bertsch, G. and Tsai, S. F. **1974**. How good is the collective model?. *Phys. Lett. B.* **50**: 319-322.
34. Ui, H. and Tsukamoto, T. **1974**. Form Factor Sum Rule and Giant Multipole States. *Prog. Theor. Phys*. **51**: 1377-1386.
35. Bohr, A. and Mottelson, B. R. **1998**. *Nuclear Structure* Vol II", World Scientific .
36. Brown, B. A., Radhi, R. and Wildenthal, B. H. **1983**. Electric quadrupole and hexadecupole nuclear excitations from the perspectives of electron scattering and modern shell-model theory. *Phys. Rep*. **101**: 313-358.
37. Chandra, H. and Sauer, G. **1976**. Relativistic corrections to the elastic electron scattering from ^{208}Pb. *Phys. Rev. C,* **13**: 245-252.
38. Wang, M., Audi, G., Wapstra, A.H., Kondev, F.G., MacCormick, M., Xu, X. and Pfeiffer, B. **2012**. The AME2012 atomic mass evaluation. *Chinese Physics C,* **36**: 1603-2014.
39. Blank, B., Marchand, C., Pravikoff, M. S., Baumann, T., Bou, F., Geissel, H., Hellström, M., Iwasa, N., Schwab, W., Sammerer, K. and Gai, M. **1997**. Total interaction and proton-removal cross-section measurements for the proton-rich isotopes ^{7}Be, ^{8}B, and ^{9}C. *Nucl. Phys*. A**, 624**: 242-256.
40. Chandel, S. S., Dhiman, S. K. and Shyam, R. **2003**. Structure of ^{8}B and astrophysical S_{17} factor in Skyrme Hartree-Fock theory. *Phys. Rev. C,* **68**: 054320.
41. Angeli, I. and Marinova, K. P. **2013**. Table of experimental nuclear ground state charge radii: An update. *Atomic Data and Nuclear Data Tables*, **99**: 69-95.
42. Riisager, K. **2013**. Halos and related structures. *Phys. Scr*. **T 152**: 014001.
43. Takechi, M. , Fukuda, M., Mihara, M., Chinda, T., Matsumasa, T., Matsubara, H., Nakashima, Y., Matsuta, K., Minamisono, T., Koyama, R., Shinosaki, W. , Takahashi, M., Takizawa, A., Ohtsubo, T., Suzuki, T., Izumikawa, T., Momota, S., Tanaka, K., Suda, T., Sasaki, M., Sato, S. and Kitagawa**,** A. **2005**. Reaction cross-sections for stable nuclei and nucleon density distribution of proton drip-line nucleus ^{8}B. *Eur. Phys. J. A,* **25**: 217-219.
44. Tanaka, K., Fukuda, M., Mihara, M., Takechi, M., Chinda, T., Sumikama, T., Kudo, S., Matsuta, K., Minamisono, T., Suzuki, T. , Ohtubo, T., Izumikawa, T., Momota, S., Yamaguchi, T., Onishi, T., Ozawa, A., Tanihata, I. and Tao, Z. **2005** . Nucleon density distribution of proton-drip nucleus ^{17}Ne". *Eur. Phys. J. A,* **25**: 221-222.
45. Warburton, E.K. and Brown, B.A. **1992**. Effective interactions for the 0*p*1*s*0*d* nuclear shell-model space". *Phys. Rev. C,* **46**: 923.
46. Stone N. J. **2014**. Table of nuclear magnetic dipole and electric quadrupole moments. IAEA, INDC(NDS)-0658, Distr. ND.
47. Cichocki, A., Dubach, J., Hicks, R. S., Peterson, G. A., De Jager, C. W., De Vries, H., Kalantar – Nayestanaki, N. and Sato, T. **1995**. Electron scattering from ^{10}B. *Phys. Rev. C,* **51**: 2406-2426.
48. Stovall, T., Goldemberg, J. and Isabelle, D. B. **1966**. Coulomb form factors of ^{10}B and ^{11}B. *Nucl. Phys. A,* **86**: 225.
49. Knight, E. A., Singhal, R. P., Arthur, R. G. and Macauley, M. W. S. **1981**. Elastic scattering of electrons from 20,22Ne". *Journal of Physics G,* **7**: 1115.